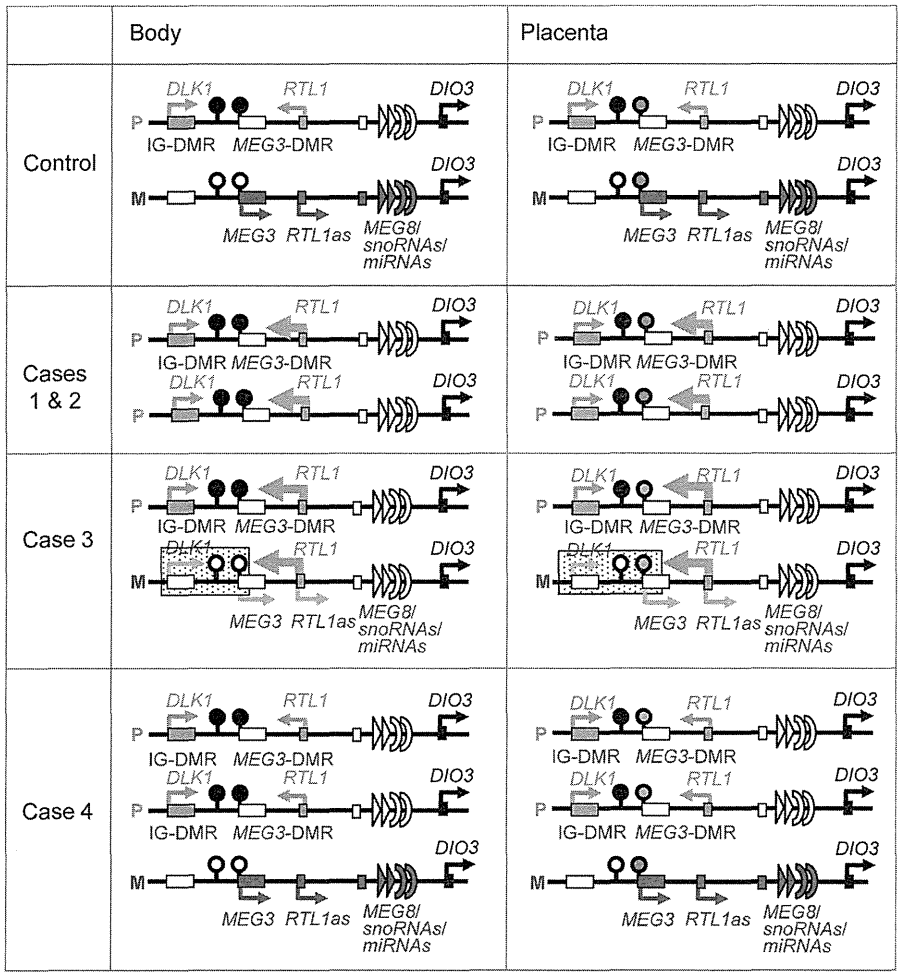

Figure 6. Schematic representation of the chromosome 14q32.2 imprinted region in a control subject, cases 1 and 2 with upd(14)pat, case 3 with a microdeletion (indicated by stippled rectangles), and case 4 with two copies of the imprinted region of paternal origin and a single copy of the imprinted region of maternal origin. This figure has been constructed using the present results and the previous data.[2,3] P, paternally derived chromosome; M, maternally derived chromosome. Filled and open circles represent hypermethylated and hypomethylated DMRs, respectively; since the *MEG3*-DMR is grossly hypomethylated and regarded as non-DMR in the placenta, it is painted in gray. *PEGs* (*DLK1* and *RTL1*) are shown in blue, *MEGs* (*MEG3*, *RTL1as*, *MEG8*, *snoRNAs* and *miRNAs*) in red, a probably non-imprinted gene (*DIO3*) in black, and non-expressed genes in white. Thick arrows for *RTL1* in cases 1–3 represent increased *RTL1* expression that is ascribed to loss of functional microRNA-containing *RTL1as* as a repressor for *RTL1*.

the *MEG3*-DMR, and FISH analyses for the 14q32.2 region were performed as described previously.[2,3] For FISH analysis of 17p13.3, a 17p sub-telomere probe and an RP11–411G7 probe for the 17p13.3 region were utilized, together with a CEP17 probe for the 17p11.1 region utilized as an internal control. The 17p sub-telomere probe was detected according to the manufacture's protocol, the RP11–411G7 probe was labeled with digoxigenin and detected by rhodamine anti-digoxigenin, and the CEP17 control probe was labeled with biotin and detected by avidin conjugated to fluorescein isothiocyanate. Quantitative real-time PCR analysis was performed on an ABI PRISM 7000 (Applied Biosystems) using TaqMan real-time PCR probe primer mixture for the following genes (assay No: Hs00171584 for *DLK1*, Hs00292028 for *MEG3*, Hs00419701 for *MEG8* and Hs00704811 for *DIO3*; assay ID: 001028 for *miR433* and 000452 for *miR127*). For *RTL1*, q-PCR analysis was performed with a forward primer hybridized to the sequence of *RTL1* and a reverse primer hybridized to the adaptor sequence. Fifty nanongrams of cDNA in a 50 μl reaction mixture contacting 2× KOD FX buffer (Toyobo), 2.0 mM dNTP mixture (Toyobo), KOD FX (Toyobo), SYBR Green I (Invitrogen), and primer set for *RTL1* were subjected to the ABI PRISM 7000. Data were normalized against *GAPDH* (catalog No: 4326317E) for *DLK1*, *MEG3*, *MEG8*, *RTL1*, and *DIO3*, and against *RNU48* (assay ID: 0010006) for *microRNAs*. The expression studies were performed three times for each sample. Oligoarray CGH was performed using 1× 1M format Human Genome Array (Catalog No G4447A) (Agilent Technologies).

Histopathological analysis. Placental samples were fixed with 20% buffered formaldehyde at room temperature and embedded in paraffin wax according to standard protocols for LM examinations. Then, sections of 3 μm thick were stained with hematoxylin-eosin. For EM examinations, fresh placental tissues were fixed with phosphate-buffered 2.5% glutaraldehyde, postfixed in 1% osmium tetroxide, and embedded in Epon 812 (catalog No. R3245, TAAB). Semithin sections were stained with 1% methylene blue, and ultrathin sections were double-stained with uranyl acetate and lead citrate. Subsequently, they were examined with a Ninhon Denshi JEM-1230 electron microscope.

For IHC analysis, sections of 3 μm thick were prepared by the same methods utilized for the LM examinations, and were examined with rabbit anti human DLK1 polyclonal antibody at 1:100 dilutions (catalog No 10636-1-AP, ProteinTech Group), rabbit anti human RTL1 polyclonal antibody at 1:200 dilutions, and rabbit anti human DIO3 polyclonal antibody at 1:50 dilutions (catalog No ab102926, abcam); anti human RTL1 polyclonal antibody was produced by immunizing rabbits with the synthesized RTL1 peptide (NH2-RGFPRDPSTESG-COOH) in this study. Sections were dewaxed in xylene and rehydrated through graded ethanol series and, subsequently, incubated in 10% citrate buffer (pH 6.0) for 40 min in a 98°C water bath, for antigen retrieval. Endogenous peroxidase activity was quenched with 1% H_2O_2 and 100% methanol for 20 min. To prevent non-specific background staining, sections are incubated with Protein Block Serum-Free (Dako corporation) for 10 min at room temperature. Then, sections were incubated overnight with primary antibody at 4°C

and, subsequently, treated with the labeled polymer prepared by combining amino acid polymers with peroxidase and anti-rabbit polyclonal antibody (Histofine Simple Stain MAX PO MULTI, Nichirei). Peroxidase activities were visualized by diaminobenzidine staining, and the nuclei were stained with hematoxylin.

Disclosure of Potential Conflicts of Interest

No potential conflicts of interest were disclosed.

Acknowledgments

This work was supported by Grants-in-Aid for Scientific Research (A) (22249010) and Research (B) (21028026) from the Japan Society for the Promotion of Science (JSPS), by Grants-in-Aid for Scientific Research on Innovative Areas (22132004-A04) from the Ministry of Education, Culture, Sports, Science and Technology (MEXT), by Grants for Research on Intractable Diseases (H22–161) from the Ministry of Health, Labor and Welfare (MHLW), by Grant for National Center for Child Health and Development (23A-1), and by Grant from Takeda Science Foundation and from Novartis Foundation.

Supplemental Materials

Supplemental materials may be found here:
www.landesbioscience.com/journals/epigenetics/article/21937

References

1. da Rocha ST, Edwards CA, Ito M, Ogata T, Ferguson-Smith AC. Genomic imprinting at the mammalian Dlk1-Dio3 domain. Trends Genet 2008; 24:306-16; PMID:18471925; http://dx.doi.org/10.1016/j.tig.2008.03.011.
2. Kagami M, Sekita Y, Nishimura G, Irie M, Kato F, Okada M, et al. Deletions and epimutations affecting the human 14q32.2 imprinted region in individuals with paternal and maternal upd(14)-like phenotypes. Nat Genet 2008; 40:237-42; PMID:18176563; http://dx.doi.org/10.1038/ng.2007.56.
3. Kagami M, O'Sullivan MJ, Green AJ, Watabe Y, Arisaka O, Masawa N, et al. The IG-DMR and the MEG3-DMR at human chromosome 14q32.2: hierarchical interaction and distinct functional properties as imprinting control centers. PLoS Genet 2010; 6:e1000992; PMID:20585555; http://dx.doi.org/10.1371/journal.pgen.1000992.
4. Kagami M, Yamazawa K, Matsubara K, Matsuo N, Ogata T. Placentomegaly in paternal uniparental disomy for human chromosome 14. Placenta 2008; 29:760-1; PMID:18619672; http://dx.doi.org/10.1016/j.placenta.2008.06.001.
5. Lin SP, Youngson N, Takada S, Seitz H, Reik W, Paulsen M, et al. Asymmetric regulation of imprinting on the maternal and paternal chromosomes at the Dlk1-Gtl2 imprinted cluster on mouse chromosome 12. Nat Genet 2003; 35:97-102; PMID:12937418; http://dx.doi.org/10.1038/ng1233.
6. Sekita Y, Wagatsuma H, Nakamura K, Ono R, Kagami M, Wakisaka N, et al. Role of retrotransposon-derived imprinted gene, Rtl1, in the feto-maternal interface of mouse placenta. Nat Genet 2008; 40:243-8; PMID:18176565; http://dx.doi.org/10.1038/ng.2007.51.
7. Lage JM. Placentomegaly with massive hydrops of placental stem villi, diploid DNA content, and fetal omphaloceles: possible association with Beckwith-Wiedemann syndrome. Hum Pathol 1991; 22:591-7; PMID:1864589; http://dx.doi.org/10.1016/0046-8177(91)90237-J.
8. Yamazawa K, Kagami M, Nagai T, Kondoh T, Onigata K, Maeyama K, et al. Molecular and clinical findings and their correlations in Silver-Russell syndrome: implications for a positive role of IGF2 in growth determination and differential imprinting regulation of the IGF2-H19 domain in bodies and placentas. J Mol Med (Berl) 2008; 86:1171-81; PMID:18607558; http://dx.doi.org/10.1007/s00109-008-0377-4.
9. Georgiades P, Watkins M, Burton GJ, Ferguson-Smith AC. Roles for genomic imprinting and the zygotic genome in placental development. Proc Natl Acad Sci U S A 2001; 98:4522-7; PMID:11274372; http://dx.doi.org/10.1073/pnas.081540898.
10. Fowden AL, Sibley C, Reik W, Constancia M. Imprinted genes, placental development and fetal growth. Horm Res 2006; 65(Suppl 3):50-8; PMID:16612114; http://dx.doi.org/10.1159/000091506.
11. Georgiades P, Ferguson-Smith AC, Burton GJ. Comparative developmental anatomy of the murine and human definitive placentae. Placenta 2002; 23:3-19; PMID:11869088; http://dx.doi.org/10.1053/plac.2001.0738.
12. Tsai CE, Lin SP, Ito M, Takagi N, Takada S, Ferguson-Smith AC. Genomic imprinting contributes to thyroid hormone metabolism in the mouse embryo. Curr Biol 2002; 12:1221-6; PMID:12176332; http://dx.doi.org/10.1016/S0960-9822(02)00951-X.
13. Yamanaka M, Ishikawa H, Saito K, Maruyama Y, Ozawa K, Shibasaki J, et al. Prenatal findings of paternal uniparental disomy 14: report of four patients. Am J Med Genet A 2010; 152A:789-91; PMID:20186803; http://dx.doi.org/10.1002/ajmg.a.33247.
14. Suzumori N, Ogata T, Mizutani E, Hattori Y, Matsubara K, Kagami M, et al. Prenatal findings of paternal uniparental disomy 14: Delineation of further patient. Am J Med Genet A 2010; 152A:3189-92; PMID:21108407; http://dx.doi.org/10.1002/ajmg.a.33719.
15. Kagami M, Kato F, Matsubara K, Sato T, Nishimura G, Ogata T. Relative frequency of underlying genetic causes for the development of UPD(14)pat-like phenotype. Eur J Hum Genet 2012; 20:928-32; PMID:22353941; http://dx.doi.org/10.1038/ejhg.2012.26.
16. Seitz H, Youngson N, Lin SP, Dalbert S, Paulsen M, Bachellerie JP, et al. Imprinted microRNA genes transcribed antisense to a reciprocally imprinted retrotransposon-like gene. Nat Genet 2003; 34:261-2; PMID:12796779; http://dx.doi.org/10.1038/ng1171.
17. Davis E, Caiment F, Tordoir X, Cavaillé J, Ferguson-Smith A, Cockett N, et al. RNAi-mediated allelic trans-interaction at the imprinted Rtl1/Peg11 locus. Curr Biol 2005; 15:743-9; PMID:15854907; http://dx.doi.org/10.1016/j.cub.2005.02.060.
18. Köhrle J. Thyroid hormone transporters in health and disease: advances in thyroid hormone deiodination. Best Pract Res Clin Endocrinol Metab 2007; 21:173-91; PMID:17574002; http://dx.doi.org/10.1016/j.beem.2007.04.001.
19. Kraus FT, Redline RW, Gersell DJ, Nelson DM, Dicker JM. Disorders of placental Development. Placental Pathology (Atlas of Noutumor Pathology). Washington, DC: American Registry of Pathology, 2004:59-68.
20. Fox HE, Sebire NJ. The placenta in abnormalities and disorders of the fetus. Pathology of the Placenta. Third edition, Philadelphia, PA: SAUNDERS, 2007:262-3.
21. Parveen Z, Tongson-Ignacio JE, Fraser CR, Killeen JL, Thompson KS. Placental mesenchymal dysplasia. Arch Pathol Lab Med 2007; 131:131-7; PMID:17227114.
22. Nakayama M. Placental pathology. Tokyo, Igaku Shoin, 2002:106-7 (in Japanese).

Mamld1 Deficiency Significantly Reduces mRNA Expression Levels of Multiple Genes Expressed in Mouse Fetal Leydig Cells but Permits Normal Genital and Reproductive Development

Mami Miyado, Michiko Nakamura, Kenji Miyado, Ken-ichirou Morohashi, Shinichiro Sano, Eiko Nagata, Maki Fukami, and Tsutomu Ogata

Departments of Molecular Endocrinology (M.M., M.N., M.F., T.O.) and Reproductive Biology (K.Mi.), National Research Institute of Child Health and Development, Tokyo 157-8535, Japan; Department of Molecular Biology (K.Mo.), Graduate School of Medical Sciences, Kyushu University, Fukuoka 812-8582, Japan; and Department of Pediatrics (S.S., E.N., T.O.), Hamamatsu University School of Medicine, Hamamatsu 431-3192, Japan

Although mastermind-like domain containing 1 (*MAMLD1*) (*CXORF6*) on human chromosome Xq28 has been shown to be a causative gene for 46,XY disorders of sex development with hypospadias, the biological function of *MAMLD1*/*Mamld1* remains to be elucidated. In this study, we first showed gradual and steady increase of testicular *Mamld1* mRNA expression levels in wild-type male mice from 12.5 to 18.5 d postcoitum. We then generated *Mamld1* knockout (KO) male mice and revealed mildly but significantly reduced testicular mRNA levels (65–80%) of genes exclusively expressed in Leydig cells (*Star*, *Cyp11a1*, *Cyp17a1*, *Hsd3b1*, and *Insl3*) as well as grossly normal testicular mRNA levels of genes expressed in other cell types or in Leydig and other cell types. However, no demonstrable abnormality was identified for cytochrome P450 17A1 and 3β-hydroxysteroid dehydrogenase (HSD3B) protein expression levels, appearance of external and internal genitalia, anogenital distance, testis weight, Leydig cell number, intratesticular testosterone and other steroid metabolite concentrations, histological findings, *in situ* hybridization findings for *sonic hedgehog* (the key molecule for genital tubercle development), and immunohistochemical findings for anti-Müllerian hormone (Sertoli cell marker), HSD3B (Leydig cell marker), and DEAD (Asp-Glu-Ala-Asp) box polypeptide 4 (germ cell marker) in the KO male mice. Fertility was also normal. These findings imply that *Mamld1* deficiency significantly reduces mRNA expression levels of multiple genes expressed in mouse fetal Leydig cells but permits normal genital and reproductive development. The contrastive phenotypic findings between *Mamld1* KO male mice and *MAMLD1* mutation positive patients would primarily be ascribed to species difference in the fetal sex development. **(*Endocrinology* 153: 6033–6040, 2012)**

Mastermind-like domain containing 1 (*MAMLD1*) (alias *CXORF6*) on human chromosome Xq28 is a causative gene for 46,XY disorders of sex development (DSDs) with hypospadias as a salient clinical phenotype. Indeed, several pathologic nonsense and frameshift mutations (p.E124X, p.Q197X, p.R653X, and p.E109fsX121) have been identified in patients with various types of hypospadias with and without other associated genital abnormalities, such as micropenis and cryptorchidism (1–3). In addition, a specific polymorphism(s) and a haplotype of *MAMLD1* appear to constitute a genetic risk factor for hypospadias (2, 4, 5).

To date, several important findings have been revealed for *MAMLD1* and its mouse homolog *Mamld1*. First, the

ISSN Print 0013-7227 ISSN Online 1945-7170
Printed in U.S.A.

doi: 10.1210/en.2012-1324 Received March 21, 2012. Accepted September 20, 2012.
First Published Online October 18, 2012

Abbreviations: Ab, Antibody; AGD, anogenital distance; AGI, AGD index; CYP17A1, cytochrome P450 17A1; dpc, days postcoitum; DSD, disorder of sex development; HSD3B, 3β-hydroxysteroid dehydrogenase; KO, knockout; *MAMLD1*, mastermind-like domain containing 1; MLTC, mouse Leydig tumor cell; *Shh*, *sonic hedgehog*; siRNA, small interfering RNA; T, testosterone; WT, wild type.

upstream region of *MAMLD1/Mamld1* harbors a putative binding site for *NR5A1* (alias *SF-1* and *AD4BP*) (6) that regulates the transcription of a vast array of genes involved in sex development (7). Second, nuclear receptor subfamily 5, group A, member 1 protein can bind to the putative target site and exert a transactivation function for *Mamld1* (6). Third, *Mamld1* is clearly coexpressed with mouse *Nr5a1* in fetal Leydig and Sertoli cells in the fetal testis (1). Fourth, transient *Mamld1* knockdown using small interfering RNAs (siRNAs) significantly reduces *Cyp17a1* expression (8) and testosterone (T) production in cultured mouse Leydig tumor cells (MLTCs) (6, 8). These findings imply that *MAMLD1/Mamld1* is involved in the molecular network for T production probably via the transactivation of *CYP17A1/Cyp17a1* under the regulation of *NR5A1* and that *MAMLD1* mutations result in 46,XY DSD phenotype with hypospadias primarily because of compromised, but not abolished, T production around the critical period for sex development.

However, the biological function of *MAMLD1/Mamld1* during testis development remains to be elucidated. Thus, we examined testicular *Mamld1* mRNA expression pattern in wild-type (WT) male mice and performed molecular and phenotypic analyses in *Mamld1* knockout (KO) male mice.

Materials and Methods

WT and *Mamld1* KO male mice

We examined WT male mice of the C57BL/6 strain purchased from Sankyo Labo Service Corp., Inc. (Tokyo, Japan) and *Mamld1* KO male mice generated by Macrogen, Inc. (Seoul, Korea). This study was approved by the Animal Ethics Committee of National Research Institute for Child Health and Development.

Mamld1 KO male mice were produced by a standard gene-targeting procedure (9). In brief, a targeting vector was designed to replace *Mamld1* exon 3, which harbors a translation start codon and approximately two thirds of the coding sequence, with a *PGK-neo* cassette (Fig. 1A). After transfection of the targeting vector into 129/Sv embryonic stem cells by electroporation, two clones of recombination-positive embryonic stem cells were selected by Southern blot analysis using probes at the 5′ and 3′ flanking regions of *Mamld1* and injected into blastocysts. The blastocysts were then transferred into pseudopregnant ICR female mice, to generate chimeric male mice. The chimeric male mice were mated with C57BL/6 female mice, and germline transmission of the mutant gene was confirmed by Southern blot analysis. Subsequently, *Mamld1* KO male mice were produced by mating heterozygous (+/−) female mice with WT male mice. The *Mamld1* KO mouse strain was backcrossed with the C57BL/6 strain and maintained for multiple generations by cross-mating between heterozygous (+/−) female mice and WT male mice.

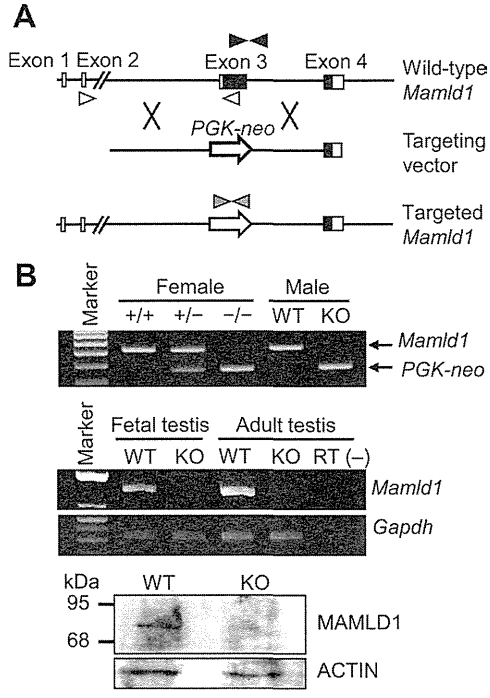

FIG. 1. Generation of *Mamld1* KO mice. A, Schematic representation of the gene targeting procedure. Exon 3 of WT *Mamld1* was replaced by the *PGK-neo* cassette (*PGK-neo*) through homologous recombination indicated by *cross symbols*. The *black and white boxes* denote the coding regions and the untranslated regions, respectively. *Paired black, white, and gray arrowheads* indicate the primer set for amplification of WT *Mamld1* genomic sequence, that for amplification of *Mamld1* transcripts, and that for amplification of Neomycin-resistant gene. B, Confirmation of *Mamld1* KO. Genotyping analysis (*upper panel*), RT-PCR analysis (*middle panel*), and Western blot analysis (*lower panel*) are consistent with successful *Mamld1* KO. +/+, WT female mice; +/−, heterozygous female mice; −/−, homozygous female mice; RT (−), negative control without reverse transcriptase.

In this study, KO male mice of the ninth generation were examined. The noon of the day when a vaginal plug was observed was designated 0.5 d postcoitum (dpc). PCR-based genotyping analysis with tail tissue genomic DNA was performed for *Mamld1*, *PGK-neo*, and *Sry*, using primers shown in Supplemental Table 1, published on The Endocrine Society's Journals Online web site at http://endo.endojournals.org. Body weight and testis weight were measured at birth.

Genital and testicular sample preparation

In the male mice, androgen synthesis starts after approximately 13.5 dpc (10, 11), and morphological characteristics of the male external genitalia are established around 16.5 dpc (12, 13). Thus, genital and testicular samples were prepared from genotype- and embryonic day-matched KO male mice and their WT littermates in the latter half of the fetal life and at birth.

Real-time RT-PCR analyses

Testes from three mice were pooled in a single tube, and five tubes were prepared for each embryonic day. Total RNA was extracted from homogenized samples using ISOGEN (Nippongene, Tokyo, Japan), and cDNA was synthesized from 200 ng of total RNA using High Capacity cDNA Reverse Transcription kit (Life Technologies, Carlsbad, CA). Real-time RT-PCR was per-

formed for *Mamld1* and 17 genes involved in sex development and expressed in the fetal testis (*Amh*, *Ar*, *Arx*, *Cyp11a1*, *Cyp17a1*, *Ddx4*, *Dhh*, *Dlx5*, *Dlx6*, *Gata4*, *Hsd17b3*, *Hsd3b1*, *Insl3*, *Nr5a1*, *Ptch1*, *Sox9*, and *Star*) as well as *Gapdh* used as an internal control, using the ABI 7500 Fast real-time PCR system (Life Technologies) and TaqMan gene expression assay kit. Primers and probes used are shown in Supplemental Table 2.

Western blot analysis

Testes collected as described above were homogenized, diluted in Laemmli buffer, and heated at 95 C. Protein extracts were subjected to a standard SDS-PAGE (12% gel) and were hybridized with anti-MAMLD1-antibody (Ab), anti-cytochrome P450 17A1(CYP17A1)-Ab, and anti-3β-hydroxysteroid dehydrogenase (HSD3B)-Ab, as well as anti-ACTIN-Ab (A2066; Sigma, St. Louis, MO) used as an internal control. Anti-MAMLD1-Ab was generated against mouse MAMLD1 peptide (CGSESFLPGSSFAHE) using rabbits, anti-CYP17A1-Ab was purchased from Santa Cruz Biotechnology, Inc. (sc-46081; Santa Cruz, CA), and anti-HSD3B-Ab was as reported previously (14). Chemiluminescence signals were detected using ECL Plus Western Blot Detection kit (GE Healthcare UK Ltd., Buckinghamshire, UK), and signal densities were assessed using an Odyssey Infrared Imaging System (LI-COR Biosciences, Lincoln, NE).

Stereoscopic observation

Morphological findings of external and internal genital regions were examined, as were anogenital distance (AGD) (the distance between the anus and the penoscrotal junction) and AGD index (AGI) (AGD divided by body weight) as indicators for the androgen action during the embryonic period (15–17). Furthermore, whole mount *in situ* hybridization was performed for *sonic hedgehog* (*Shh*), one of the key molecules for the development of genital tubercle (18, 19), using an antisense cRNA fragment as a probe (GenBank accession no. BC063087; nucleotide position, 138-1499). Sense cRNA was used as a negative control. Hybridization was performed using the Wilkinson procedure (20), and signals were visualized with the BM Purple AP Substrate (Roche, Mannheim, Germany).

Histological and immunohistochemical examinations

Histological examination was performed for tissue samples that were fixed with 4% paraformaldehyde, dehydrated, and embedded in paraffin. Serial 6-μm sections were mounted on Superfrost slides, and every tenth section was stained with hematoxylin-eosin.

Immunohistochemical examination was carried out for the remaining section slides that were deparaffinized and incubated with 3% H_2O_2 in PBS to inactivate endogenous peroxidases. The slides were then incubated in blocking solution (Roche) and transferred into a new solution containing polyclonal primary Abs against anti-Mülerian hormone (sc-46081; Santa Cruz Biotechnology, Inc.) as a marker for Sertoli cells, HSD3B as a marker for Leydig cells, DEAD (Asp-Glu-Ala-Asp) box polypeptide 4 (ab13840; Abcam, Cambridge, UK) as a marker for germ cells, and proliferating cell nuclear antigen (PC10; Dako, Glostrup, Denmark) as a marker for proliferating cells. The samples were washed and incubated with secondary Abs conjugated with horseradish peroxidase (Santa Cruz Biotechnology, Inc.). The Simple Stain DAB Solution (Nichirei, Tokyo, Japan) was used for color development. Apoptotic cells were detected by terminal deoxynucleotidyl transferase 2′-deoxyuridine, 5′-triphosphate nick end labeling staining using an *In Situ* Apoptosis Detection kit (TaKaRa Bio, Shiga, Japan). Furthermore, HSD3B-positive cells in four randomly selected fields of each testis were counted, to estimate the number of Leydig cells.

Measurement of intratesticular T and steroid metabolites

Intratesticular T and steroid metabolites were measured at 18.5 dpc by liquid chromatography tandem mass spectrometry (ASKA Pharma Medical, Kanagawa, Japan) using samples stored at −80 C, because intratesticular T usually peaks at 18.5 dpc in normal mice (10, 11).

Cross-mating experiments

Cross-mating was performed between *Mamld1* KO male mice and WT or heterozygous (+/−) female mice and between WT male mice and WT or heterozygous (+/−) female mice.

Statistical analysis

The data are expressed as the mean ± SEM. Statistical significance of the mean between two groups was examined by Student's *t* test, and that of the frequency between two groups was examined by χ^2 test. $P < 0.05$ was considered significant.

Results

Mamld1 expression in the fetal testis of WT male mice

Real-time RT-PCR analyses indicated a gradual and steady increase in the *Mamld1* mRNA levels from 12.5 to 18.5 dpc (Fig. 2).

Generation of *Mamld1* KO male mice

Mamld1 KO male mouse was successfully produced. *Mamld1* exon 3 was deleted from the genome of the KO

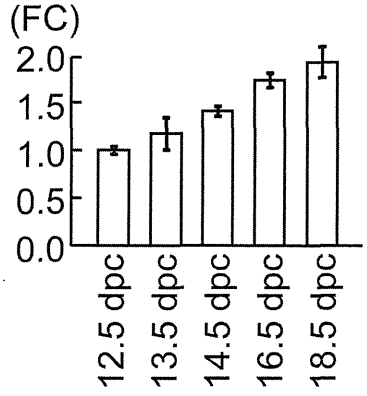

FIG. 2. Testicular *Mamld1* expression levels during the latter half of the fetal life in WT male mice. Figure indicates the data obtained by real-time RT-PCR analyses. Fold change (FC) represents relative mRNA levels of *Mamld1* against *Gapdh*. The relative expression level of *Mamld1* mRNA at 12.5 dpc was designated as 1.0.

TABLE 1. Comparison between *Mamld1* KO mice and their WT littermates

	KO	WT	*P* value
Body weight (g) (at birth)	1.48 ± 0.03 (n = 10)	1.44 ± 0.03 (n = 10)	0.40
AGD (mm) (at birth)	1.33 ± 0.02 (n = 10)	1.32 ± 0.02 (n = 10)	0.62
AGI (mm/g) (at birth)	0.90 ± 0.02 (n = 10)	0.92 ± 0.02 (n = 10)	0.55
Leydig cells (HSD3B-stained cells) (number/HPF) (at 14.5 dpc)	69.3 ± 8.2 (n = 3)	75.1 ± 7.6 (n = 3)	0.63
Testis weight (mg) (at birth)	1.46 ± 0.08 (n = 10)	1.35 ± 0.08 (n = 10)	0.34
Intratesticular steroid metabolites (at 18.5 dpc)			
Pregnenolone (pg/two testes)	17.9 ± 4.0 (n = 4)	15.4 ± 1.4 (n = 4)	0.57
Progesterone (pg/two testes)	16.5 ± 4.6 (n = 4)	15.0 ± 1.7 (n = 4)	0.56
17-OH pregnenolone (pg/two testes)	15.2 ± 2.9 (n = 4)	15.4 ± 1.3 (n = 4)	0.77
17-OH progesterone (pg/two testes)	10.4 ± 1.7 (n = 4)	13.5 ± 2.5 (n = 4)	0.15
Androstenedione (ng/two testes)	0.44 ± 0.15 (n = 4)	0.51 ± 0.07 (n = 4)	0.25
T (ng/two testes)	2.31 ± 0.30 (n = 4)	2.38 ± 0.31 (n = 4)	0.89

Expressed as mean ± SEM. HPF, High power field (234.1 × 175.5 μm).

mice, and neither *Mamld1* mRNA nor MAMLD1 protein was identified in the testis of the KO mice (Fig. 1B). Body weight was comparable between the KO male mice and their WT littermates (Table 1).

Gene and protein expression pattern in the fetal testes of *Mamld1* KO mice

The results are shown in Fig. 3. Relative mRNA levels of *Cyp17a1*, *Hsd3b1*, and *Insl3* mRNAs were mildly but

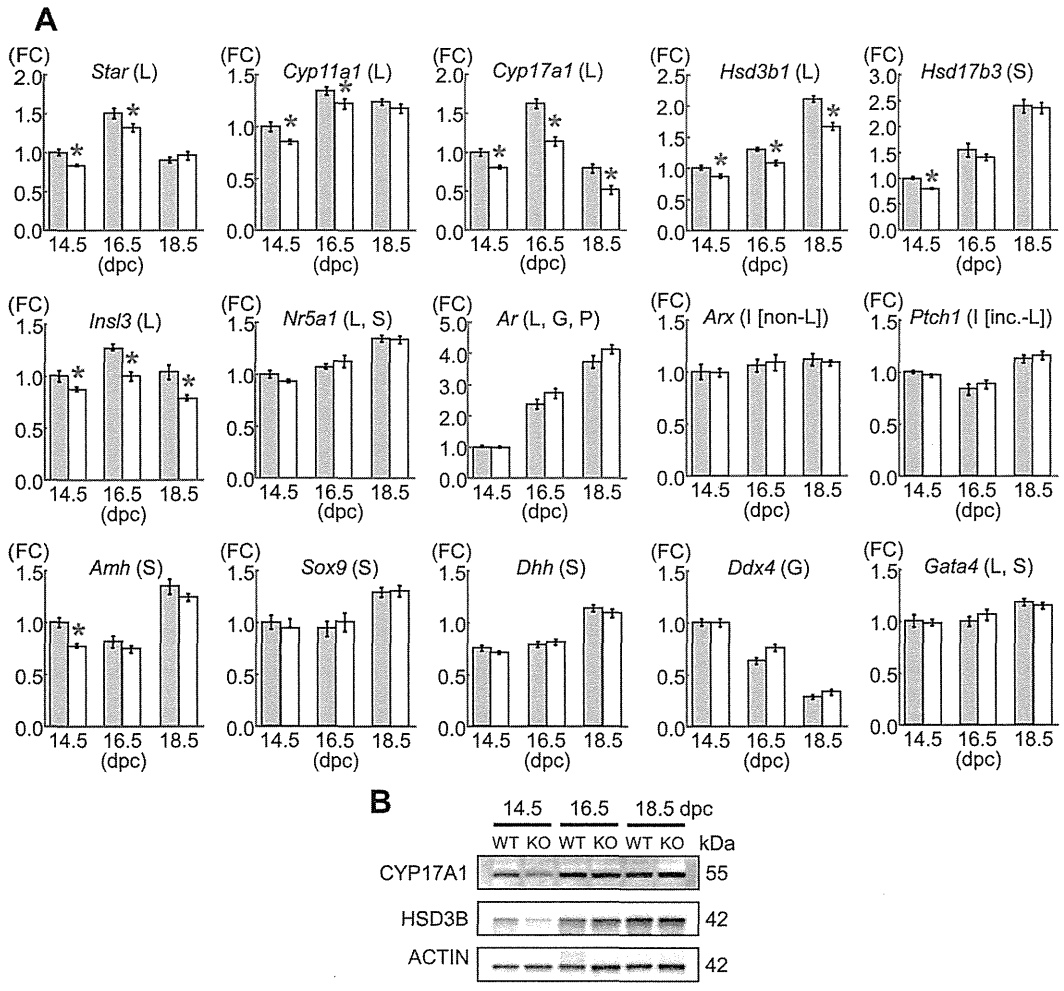

FIG. 3. Gene and protein expression patterns in the fetal testes. A, Relative mRNA levels of examined genes against *Gapdh*. FC, Fold change; L, Leydig cells; S, Sertoli cells; G, germ cells; P, peritubular cells; I [non-L], interstitial cells excluding Leydig cells; I [inc.-L], interstitial cells including Leydig cells. The *green and the yellow bars* indicate the data obtained from WT male mice and *Mamld1* KO male, respectively. For each gene, the relative expression level of mRNA in WT male mice at 14.5 dpc was designated as 1.0. *Red asterisks* indicate significant results ($P < 0.05$). B, Western blot analysis for CYP17A1 and HSD3B, as well as for ACTIN.

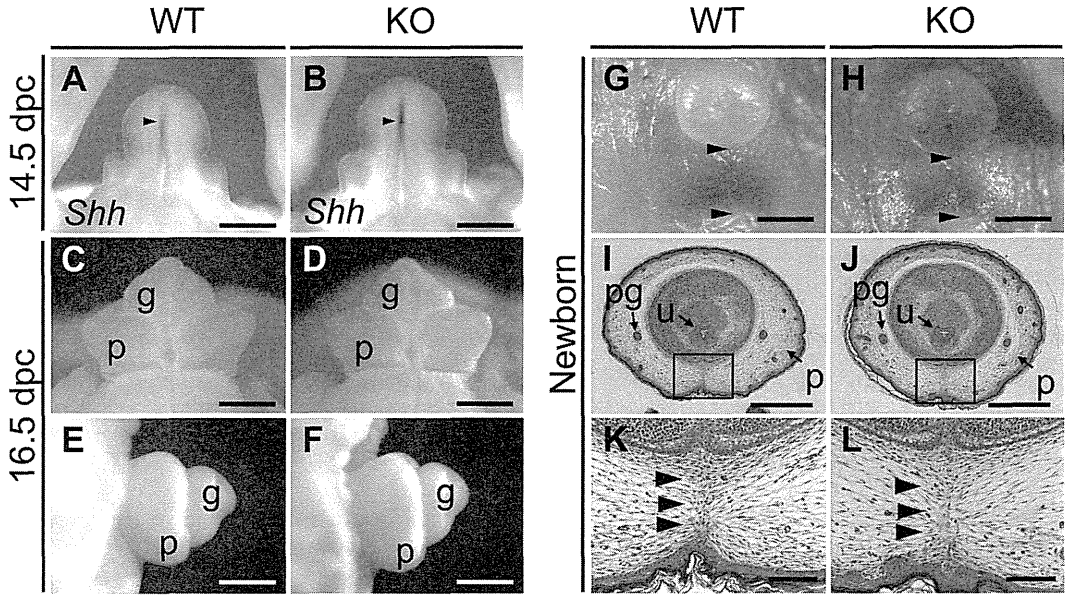

FIG. 4. External genitalia of WT and *Mamld1* KO male mice. A and B, Whole mount *in situ* hybridization for *Shh* (*arrowheads*) in the developing genital region at 14.5 dpc. C–F, Appearance of the genital tubercle at 16.5 dpc. G and H, Appearance of the external genitalia at birth. The distance between the anus and the penoscrotal junction (*arrowheads*) represents the AGD. I–L, Histological findings of the external genitalia at birth. *Arrowheads* in K and L indicate the fused prepuce. g, Glans; p, prepuce; pg, preputal gland; u, urethra. *Scale bars*: 500 μm (A–F, I, and J), 1 mm (G and H), and 100 μm (K and L).

significantly lower in the KO male mice than in their WT littermates at 14.5, 16.5, and 18.5 dpc, as were those for *Star* and *Cyp11a1* at 14.5 and 16.5 dpc (65–80%) (*Dlx5* and *Dlx6* expression levels were extremely low). By contrast, relative mRNA levels of the remaining genes were comparable between the KO male mice and their WT littermates, except for relative mRNA levels of *Hsd17b3* and *Amh* at 14.5 dpc. However, expression levels of CYP17A1 and HSD3B proteins were similar between the KO male mice and their WT littermates and were obviously higher at 16.5 and 18.5 dpc than at 14.5 dpc.

External genital findings of *Mamld1* KO male mice

External genitalia were obviously normal in the *Mamld1* KO male mice (Fig. 4 and Table 1). *Shh* was normally expressed in the urethral epithelium of the KO male mice at 14.5 dpc, and subsequent outgrowth of genital tubercle and fusion of the urethral folds at the ventral midline occurred in the KO male mice at the same embryonic stages as in their WT littermates. Furthermore, external genitalia were normally developed at birth, with the comparable AGD and AGI between the KO mice and their WT littermates.

Internal genital findings of *Mamld1* KO mice

Internal genitalia of the *Mamld1* KO male mice were also free from demonstrable abnormality (Fig. 5 and Table 1). Intraabdominal testicular descent, wolffian development, and müllerian regression were normally observed in the KO male mice at 16.5 dpc. Testicular histological findings were comparable between the KO mice and their WT littermates at 14.5 dpc and at birth. Immunohistochemical findings indicated the presence of similar numbers of Sertoli cells (anti-Müllerian hormone-stained cells), Leydig cells (HSD3B-stained cells), and germ cells [DEAD (Asp-Glu-Ala-Asp) box polyoeotide 4-stained cells] at 14.5 dpc as well as the presence of a similar number of Leydig cells (HSD3B-stained cells) at birth between the KO mice and their WT littermates. A relatively large number of mitotic cells (proliferating cell nuclear antigen-stained cells) was also identified in both the KO mice and their WT littermates, as were a small number of apoptotic cells (terminal deoxynucleotidyl transferase 2′-deoxyuridine, 5′-triphosphate nick end labeling-stained cells) (data not shown). In addition, testis weights at birth and intratesticular concentrations of T and other steroid metabolites at 18.5 dpc were also similar between the KO mice and their WT littermates.

Cross-mating experiments

The results are shown in Table 2. *Mamld1* KO male mice produced offspring with WT and heterozygous (+/−) female mice, as did WT male mice. Furthermore, the frequency of littermate offspring [*Mamld1* KO male mice, WT male mice, homozygous (−/−) female mice, heterozygous (+/−) female mice, and WT female mice] was in agreement with the expected Mendelian mode of inheritance.

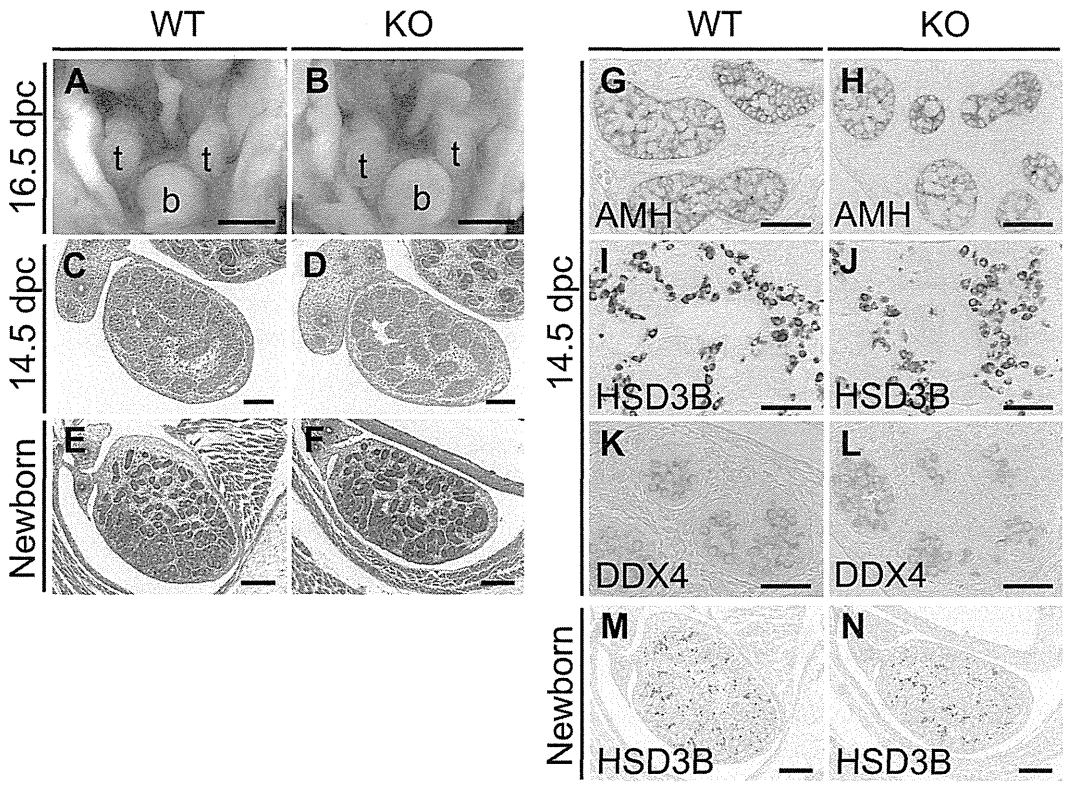

FIG. 5. Internal genitalia of WT and *Mamld1* KO male mice. A and B, Appearance of internal genital organs at 16.5 dpc. C–F, Histological findings of testes at 14.5 dpc and birth. G–N, Immunohistochemical findings of testes at 14.5 dpc and birth. b, Bladder; t, testis. *Scale bars*: 1 mm (A and B), 100 μm (C and D), 200 μm (E, F, M, and N), and 50 μm (G–L).

Discussion

The *Mamld1* mRNA expression was gradually and steadily increased from 12.5 to 18.5 dpc in the fetal testis of WT male mice. In this regard, intratesticular T has also been reported to increase in a similar manner in the mouse (10, 11). In addition, human study has also revealed clear *MAMLD1* expression in the fetal testis. These findings would argue for a positive role of *MAMLD1/Mamld1* in the T production in the fetal testis (1, 21).

We generated and studied *Mamld1* KO male mice. The results are summarized as follows: 1) mRNA levels of genes exclusively expressed in Leydig cells (*Star*, *Cyp11a1*, *Cyp17a1*, *Hsd3b1*, and *Insl3*) were mildly but significantly reduced, whereas those of genes expressed in other cell types or in Leydig and other cell types grossly remained normal (*Hsd17b3* is expressed in Sertoli cells of the fetal testis, although it is expressed in Leydig cells of the adult testis) (22, 23); 2) despite such mild reduction of mRNA levels, CYP17A1 and HSD3B proteins were sufficiently produced; 3) no demonstrable abnormality was identified by detailed studies for the external and internal genital regions; and 4) the *Mamld1* KO male mice retained normal fertility. Collectively, these findings imply that *Mamld1* deficiency reduces mRNA expression levels of multiple, if not all, genes expressed in mouse fetal Leydig cells but permits normal genital development and reproductive function. In support of this notion, such discrepancy between mRNA levels and protein levels as well as phenotypic consequences has been reported previously (24–26). Indeed, Greenbaum *et al.* (27) have proposed three possible explanations for the poor correlations between mRNA and protein expression levels: 1) there are many complicated and varied posttranscriptional mechanisms involved in turning mRNA into protein that are not yet sufficiently well defined; 2) proteins may differ substantially in their *in vivo* half lives; and 3) there may be a significant amount of error and noise in both protein and mRNA experiments that limit our ability to get a clear picture. These explanations would also apply to our results indicating normal expression of CYP17A1 and HSD3B proteins, in the presence of mildly but significantly reduced expression of *Cyp17a1* and *Hsd3b1* mRNAs. Furthermore, because CYP17A1 and HSD3B protein levels increased in a manner grossly similar to that reported for intratesticular T (10, 11) in both the *Mamld1* KO male mice and their WT littermates, this would be consistent with the apparently normal testicular function of the *Mamld1* KO male mice.

The normal phenotype in the *Mamld1* KO male mice is contrastive to the DSD phenotype in the *MAMLD1* mu-

TABLE 2. Cross-mating experiments for *Mamld1*

Offspring produced by cross-mating between *Mamld1* KO male mice (n = 5) and WT female mice (n = 24)					
Sex and *Mamld1* genotype	Male (−)	Male (+)	Female (−/−)	Female (+/−)	Female (+/+)
Number and frequency	n/o	89 (45.6%)	n/o	106 (54.4%)	n/o
Offspring produced by cross-mating between *Mamld1* KO male mice (n = 14) and heterozygous female mice (n = 49)					
Sex and *Mamld1* genotype	Male (−)	Male (+)	Female (−/−)	Female (+/−)	Female (+/+)
Number and frequency	84 (23.6%)	96 (27.0%)	94 (26.4%)	82 (23.0%)	n/o
Offspring produced by cross-mating between WT male mice (n = 6) and WT female mice (n = 12)					
Sex and *Mamld1* genotype	Male (−)	Male (+)	Female (−/−)	Female (+/−)	Female (+/+)
Number and frequency	n/o	58 (59.8%)	n/o	n/o	39 (40.2%)
Offspring produced by cross-mating between WT male mice (n = 9) and heterozygous female mice (n = 46)					
Sex and *Mamld1* genotype	Male (−)	Male (+)	Female (−/−)	Female (+/−)	Female (+/+)
Number and frequency	86 (25.3%)	85 (25.0%)	n/o	84 (24.7%)	85 (25.0%)

WT or +, WT; KO or −, *Mamld1* KO; n/o, not obtained.

tation positive patients (1, 3). In this regard, it is notable that male genital development is primarily induced by testicular T that is produced via Δ^5-pathway under the stimulation of chorionic gonadotropin during the first trimester in the human (28–31), whereas it is primarily carried out by testicular T that is produced via Δ^4-pathway independently of the chorionic gonadotropin stimulation during the late gestational period in the mouse (10, 31, 32). Thus, although the detailed mechanism(s) remains to be clarified, such species difference in the fetal male sex development may underlie the phenotypic difference between the *Mamld1* KO male mice and the *MAMLD1* mutation positive patients. In addition, the bias that individuals with abnormal phenotypes only are usually examined in the human study may also be relevant to this matter.

The results of mRNA expression levels and intratesticular hormone concentrations in the *Mamld1* KO male mice are different from those identified by transient *Mamld1* knockdown experiments using siRNAs and MLTCs (6, 8), although the normal Leydig cell number of the *Mamld1* KO male mice appears to be consistent with the sustained proliferation of siRNA-transfected MLTCs (8). Indeed, *Mamld1* knockdown has predominantly affected *Cyp17a1* expression (8) and significantly decreased T and other steroid metabolite after 17α-hydroxylation (6, 8). However, MLTCs are derived from adult Leydig tumor cells and are characterized by a markedly low 17α-hydroxylase activity and a well-preserved 17/20 lyase activity for both Δ^4- and Δ^5-pathways (33). Such unique properties of MLTCs may be relevant to the preferential impairment of *Cyp17a1* expression and 17α-hydroxylation in siRNA-transfected MLTCs.

Two findings also appear to be worth pointing out in this study. First, *Insl3* mRNA expression was significantly reduced and *Amh* mRNA expression was grossly normal, in the *Mamld1* KO mice. Such mRNA expression patterns, if they also take place in the human, would be relevant to the frequent occurrence of cryptorchidism and the lack of müllerian derivatives in patients with *MAMLD1* mutations (1). Second, *Mamld1* KO male mice, WT male mice, homozygous (−/−) female mice, heterozygous (+/−) female mice, and WT female mice were born with frequencies consistent with the Mendelian mode of inheritance. Thus, although *Mamld1* is ubiquitously expressed with strong expressions in the central nervous system (1), *Mamld1* deficiency is unlikely to affect viability.

In summary, the present study implies that *Mamld1* enhances mRNA expression levels of multiple genes exclusively expressed in fetal Leydig cells, although the effects of *Mamld1* deficiency are insufficient to compromise the genital and reproductive development. Further studies will permit a better clarification of the biological function of *MAMLD1/Mamld1*.

Acknowledgments

Address all correspondence and requests for reprints to: Professor Tsutomu Ogata, Department of Pediatrics, Hamamatsu University School of Medicine, Hamamatsu 431-3192, Japan. E-mail: tomogata@hama-med.ac.jp.

This work was supported by the National Center for Child Health and Development Grant 23A-1; Grant for Research on Intractable Diseases from the Ministry of Health, Labor, and

Welfare; Environment Research and Technology Development Fund C-0905 of the Ministry of Environment; Grants-in-Aid for Scientific Research (B) 23390249 and (S) 22227002 and for Young Scientists (B) 24790303 from the Japan Society for the Promotion of Science; and Grant-in-Aid for Scientific Research on Innovative Areas 22132004 from the Ministry of Education, Culture, Sports, Science, and Technology.

Disclosure Summary: The authors have nothing to disclose.

References

1. **Fukami M, Wada Y, Miyabayashi K, Nishino I, Hasegawa T, Nordenskjöld A, Camerino G, Kretz C, Buj-Bello A, Laporte J, Yamada G, Morohashi K, Ogata T** 2006 CXorf6 is a causative gene for hypospadias. Nat Genet 38:1369–1371
2. **Kalfa N, Liu B, Klein O, Ophir K, Audran F, Wang MH, Mei C, Sultan C, Baskin LS** 2008 Mutations of CXorf6 are associated with a range of severities of hypospadias. Eur J Endocrinol 159:453–458
3. **Ogata T, Laporte J, Fukami M** 2009 MAMLD1 (CXorf6): a new gene involved in hypospadias. Horm Res 71:245–252
4. **Chen Y, Thai HT, Lundin J, Lagerstedt-Robinson K, Zhao S, Markljung E, Nordenskjöld A** 2010 Mutational study of the MAMLD1-gene in hypospadias. Eur J Med Genet 53:122–126
5. **van der Zanden LF, van Rooij IA, Feitz WF, Franke B, Knoers NV, Roeleveld N** 2012 Aetiology of hypospadias: a systematic review of genes and environment. Hum Reprod Update 18:260–283
6. **Fukami M, Wada Y, Okada M, Kato F, Katsumata N, Baba T, Morohashi K, Laporte J, Kitagawa M, Ogata T** 2008 Mastermind-like domain-containing 1 (MAMLD1 or CXorf6) transactivates the Hes3 promoter, augments testosterone production, and contains the SF1 target sequence. J Biol Chem 283:5525–5532
7. **Lin L, Achermann JC** 2008 Steroidogenic factor-1 (SF-1, Ad4BP, NR5A1) and disorders of testis development. Sex Dev 2:200–209
8. **Nakamura M, Fukami M, Sugawa F, Miyado M, Nonomura K, Ogata T** 2011 Mamld1 knockdown reduces testosterone production and Cyp17a1 expression in mouse Leydig tumor cells. PLoS One 6:e19123
9. **Hogan B, Beddington R, Costantini F, Lacy E** 1994 Manipulating the mouse embryo: a laboratory manual. New York: Cold Spring Harbor Laboratory Press
10. **O'Shaughnessy PJ, Baker P, Sohnius U, Haavisto AM, Charlton HM, Huhtaniemi I** 1998 Fetal development of Leydig cell activity in the mouse is independent of pituitary gonadotroph function. Endocrinology 139:1141–1146
11. **O'Shaughnessy PJ, Baker PJ, Johnston H** 2006 The foetal Leydig cell-differentiation, function and regulation. Int J Androl 29:90–95; discussion 105–108
12. **Miyagawa S, Satoh Y, Haraguchi R, Suzuki K, Iguchi T, Taketo MM, Nakagata N, Matsumoto T, Takeyama K, Kato S, Yamada G** 2009 Genetic interactions of the androgen and Wnt/β-catenin pathways for the masculinization of external genitalia. Mol Endocrinol 23:871–880
13. **Suzuki K, Ogino Y, Murakami R, Satoh Y, Bachiller D, Yamada G** 2002 Embryonic development of mouse external genitalia: insights into a unique mode of organogenesis. Evol Dev 4:133–141
14. **Fatchiyah, Zubair M, Shima Y, Oka S, Ishihara S, Fukui-Katoh Y, Morohashi K** 2006 Differential gene dosage effects of Ad4BP/SF-1 on target tissue development. Biochem Biophys Res Commun 341:1036–1045
15. **Graham S, Gandelman R** 1986 The expression of ano-genital distance data in the mouse. Physiol Behav 36:103–104
16. **Kerin TK, Vogler GP, Blizard DA, Stout JT, McClearn GE, Vandenbergh DJ** 2003 Anogenital distance measured at weaning is correlated with measures of blood chemistry and behaviors in 450-day-old female mice. Physiol Behav 78:697–702
17. **Swan SH, Main KM, Liu F, Stewart SL, Kruse RL, Calafat AM, Mao CS, Redmon JB, Ternand CL, Sullivan S, Teague JL** 2005 Decrease in anogenital distance among male infants with prenatal phthalate exposure. Environ Health Perspect 113:1056–1061
18. **Haraguchi R, Mo R, Hui C, Motoyama J, Makino S, Shiroishi T, Gaffield W, Yamada G** 2001 Unique functions of Sonic hedgehog signaling during external genitalia development. Development 128:4241–4250
19. **Miyagawa S, Matsumaru D, Murashima A, Omori A, Satoh Y, Haraguchi R, Motoyama J, Iguchi T, Nakagata N, Hui CC, Yamada G** 2011 The role of sonic hedgehog-Gli2 pathway in the masculinization of external genitalia. Endocrinology 152:2894–2903
20. **Wilkinson D** 1992 *In situ* hybridization: a practical approach. London: Oxford University Press
21. **O'Shaughnessy PJ, Baker PJ, Monteiro A, Cassie S, Bhattacharya S, Fowler PA** 2007 Developmental changes in human fetal testicular cell numbers and messenger ribonucleic acid levels during the second trimester. J Clin Endocrinol Metab 92:4792–4801
22. **Baker PJ, Sha JH, O'Shaughnessy PJ** 1997 Localisation and regulation of 17β-hydroxysteroid dehydrogenase type 3 mRNA during development in the mouse testis. Mol Cell Endocrinol 133:127–133
23. **O'Shaughnessy PJ, Baker PJ, Heikkilä M, Vainio S, McMahon AP** 2000 Localization of 17β-hydroxysteroid dehydrogenase/17-ketosteroid reductase isoform expression in the developing mouse testis-androstenedione is the major androgen secreted by fetal/neonatal leydig cells. Endocrinology 141:2631–2637
24. **Lehmann KP, Phillips S, Sar M, Foster PM, Gaido KW** 2004 Dose-dependent alterations in gene expression and testosterone synthesis in the fetal testes of male rats exposed to di (n-butyl) phthalate. Toxicol Sci 81:60–68
25. **Thompson CJ, Ross SM, Hensley J, Liu K, Heinze SC, Young SS, Gaido KW** 2005 Differential steroidogenic gene expression in the fetal adrenal gland versus the testis and rapid and dynamic response of the fetal testis to di(n-butyl) phthalate. Biol Reprod 73:908–917
26. **Weisser J, Landreh L, Söder O, Svechnikov K** 2011 Steroidogenesis and steroidogenic gene expression in postnatal fetal rat Leydig cells. Mol Cell Endocrinol 341:18–24
27. **Greenbaum D, Colangelo C, Williams K, Gerstein M** 2003 Comparing protein abundance and mRNA expression levels on a genomic scale. Genome Biol 4:117
28. **Flück CE, Miller WL, Auchus RJ** 2003 The 17, 20-lyase activity of cytochrome p450c17 from human fetal testis favors the δ5 steroidogenic pathway. J Clin Endocrinol Metab 88:3762–3766
29. **Fowler PA, Bhattacharya S, Gromoll J, Monteiro A, O'Shaughnessy PJ** 2009 Maternal smoking and developmental changes in luteinizing hormone (LH) and the LH receptor in the fetal testis. J Clin Endocrinol Metab 94:4688–4695
30. **Huhtaniemi IT, Korenbrot CC, Jaffe RB** 1977 HCG binding and stimulation of testosterone biosynthesis in the human fetal testis. J Clin Endocrinol Metab 44:963–967
31. **Scott HM, Mason JI, Sharpe RM** 2009 Steroidogenesis in the fetal testis and its susceptibility to disruption by exogenous compounds. Endocr Rev 30:883–925
32. **Baker PJ, O'Shaughnessy PJ** 2001 Role of gonadotrophins in regulating numbers of Leydig and Sertoli cells during fetal and postnatal development in mice. Reproduction 122:227–234
33. **Panesar NS, Chan KW, Ho CS** 2003 Mouse Leydig tumor cells produce C-19 steroids, including testosterone. Steroids 68:245–251

NOTE

Advance Publication
doi: 10.1507/endocrj.EJ12-0257

Neuromuscular symptoms in a patient with familial pseudohypoparathyroidism type Ib diagnosed by methylation-specific multiplex ligation-dependent probe amplification

Keisuke Nagasaki[1), 2)*], Shuichi Tsuchiya[3)*], Akihiko Saitoh[2)], Tsutomu Ogata[1), 4)] and Maki Fukami[1)]

[1)] *Department of Molecular Endocrinology, National Research Institute for Child Health and Development, Tokyo 157-8535, Japan*
[2)] *Division of Pediatrics, Department of Homeostatic Regulation and Development, Niigata University Graduate School of Medical and Dental Sciences, Niigata 951-8510, Japan*
[3)] *Department of Pediatrics, Ojiya general Hospital, Niigata 947-8641, Japan*
[4)] *Department of Pediatrics, Hamamatsu University School of Medicine, Hamamatsu 431-3192, Japan*

Abstract. Pseudohypoparathyroidism type Ib (PHP-Ib) is a rare genetic disorder characterized by hypocalcemia and hyperphosphatemia due to imprinting defects in the maternally derived *GNAS* allele. Patients with PHP-Ib are usually identified by tetany, convulsions, and/or muscle cramps, whereas a substantial fraction of patients remain asymptomatic and are identified by familial studies. Although previous studies on patients with primary hypoparathyroidism have indicated that hypocalcemia can be associated with various neuromuscular abnormalities, such clinical features have been rarely described in patients with PHP-Ib. Here, we report a 12-year-old male patient with familial PHP-Ib and unique neuromuscular symptoms. The patient presented with general fatigue, steppage gait, and myalgia. Physical examinations revealed muscular weakness and atrophies in the lower legs, a shortening of the bilateral Achilles' tendons and absence of deep tendon reflexes. Laboratory tests showed hypocalcemia, hyperphosphatemia, elevated serum intact PTH level, and impaired responses of urinary phosphate and cyclic AMP in an Ellsworth-Howard test, in addition to an elevated serum creatine kinase level. Clinical features of the patient were significantly improved after 1 month of treatment with alfacalcidol and calcium. Methylation-specific multiplex ligation-dependent probe amplification (MS-MLPA) and subsequent PCR analyses identified a methylation defect at exon A/B of *GNAS* and a microdeletion involving exons 4-6 of the *GNAS* neighboring gene *STX16* in the patient and in his asymptomatic brother. The results suggest that various neuromuscular features probably associated with hypocalcemia can be the first symptoms of PHP-Ib, and that MS-MLPA serves as a powerful tool for screening of GNAS abnormalities in patients with atypical manifestations.

Key words: PHP-Ib, Neuromuscular symptoms, Hypocalcemia, *STX16*, MS-MLPA

PSEUDOHYPOPARATHYROIDISM (PHP; MIM 103580) is a genetically heterogeneous condition characterized by hypocalcemia and hyperphosphatemia resulting from end-organ resistance to PTH [1]. PHP is classified into 2 subtypes, PHP-Ia and -Ib, according to the molecular causes and clinical features of the patients [1]. PHP-Ia results from loss-of-function mutations in the maternally derived *GNAS* gene that encodes the stimulatory G protein α-subunit [1]. Patients with PHP-Ia manifest multiple hormone resistance and characteristic physical stigmata such as short stature, obesity, round face, brachydactyly, subcutaneous ossification, and mild to moderate mental retardation, which are collectively referred to as Albright's hereditary osteodystrophy (AHO) [1, 2].

PHP-Ib is caused by imprinting defects of the maternally derived *GNAS* allele; patients with this condi-

Submitted Jul. 17, 2012; Accepted Oct. 14, 2012 as EJ12-0257
Released online in J-STAGE as advance publication Oct. 25, 2012
Correspondence to: Keisuke Nagasaki, Division of Pediatrics, Department of Homeostatic Regulation and Development, Niigata University Graduate School of Medical and Dental Sciences, Niigata, 951-8510, Japan. E-mail: nagasaki@med.niigata-u.ac.jp
Maki Fukami, Department of Molecular Endocrinology, National Research Institute for Child Health and Development, Tokyo 157-8535, Japan. E-mail: mfukami@nch.go.jp
* K.N. and S.T. contributed equally to this work.

tion show hypomethylation at one or more of the 4 differentially methylated regions (DMRs) of *GNAS* [3-7]. Genetic causes of PHP-Ib include cryptic deletions within the genes neighboring *GNAS*, *STX16* and *NESP55*, and epimutation of *GNAS* DMRs [4, 5]. Patients with PHP-Ib manifest PTH resistance without AHO [1]. These patients are usually identified by hypocalcemia-associated neuromuscular irritability, such as tetany, generalized convulsions, and/or muscle cramps, although a substantial fraction of the patients remain asymptomatic and are identified only by familial studies [6, 7].

Previous studies of patients with primary hypoparathyroidism have shown that hypocalcemia can be associated with various types of neuromuscular symptoms [8, 9]. However, such clinical features have been rarely described in patients with PHP-Ib [10]. Here, we report a Japanese patient with familial PHP-Ib due to an intragenic deletion of *STX16*, who presented with unique neuromuscular symptoms.

Methods

Case report

This male patient was born as the third child to non-consanguineous Japanese parents at 39 weeks of gestation, after an uncomplicated pregnancy and delivery. His birth weight was 3482 g (+1.1 SD) and length 50 cm (+0.7 SD). Neonatal screening tests were normal. His postnatal growth and development were uneventful.

From the age of 6 years, he had general fatigue. At 12 years of age, he was seen by a local doctor because of general fatigue, gait disturbance, and myalgia in the lower legs. He was suspected to have congenital myopathy, and was referred to our clinic for further investigation. His height and weight at the time of examination were 161.4 cm (+1.1 SD) and 42.4 kg (-0.2 SD), respectively. Physical examinations revealed muscular atrophies with weakness in the lower legs, a shortening of the bilateral Achilles' tendons and absence of deep tendon reflexes. He showed a high stepping gait with markedly reduced strength of dorsiflexors of the ankles. Sense of touch and temperature was normal. The Chvostek's sign was positive, while the Trousseau's sign was negative. He had neither AHO stigmata nor episodes of tetany or convulsions. Laboratory examinations revealed hypocalcemia, hyperphosphatemia, and an elevated serum intact PTH level, together with decreased urinary calcium excretions (Table 1). Serum creatine kinase (CK) level was markedly elevated. An Ellsworth-Howard test showed impaired responses of both urinary phosphaturic and cyclic AMP levels (Table 1). The TSH level was slightly elevated, while free T4 and gonadotropin levels were within the normal range. The serum 1,25-dihydroxy vitamin D (1,25(OH)2D) level was mildly elevated. Head computerized tomography (CT) delineated symmetric calcifications of the basal ganglia and thalami, and subcortical calcification of the right middle frontal gyrus. Dual-energy X-ray absorptiometry (DEXA) revealed decreased bone mineral density at the lumbar spine (L2-L4) (0.640 g/cm^2, -2.9 SD). Based on these data, we diagnosed him as having PHP-Ib with neuromuscular symptoms. After 1 month of treatment with alfacalcidol (1.5 μg/day) and calcium lactate (3.0 g/day), his general fatigue, gait disturbance, and myalgia were markedly improved.

The 15-year-old brother of the patient manifested no clinically discernible phenotype; the brother had no gait disturbance or muscle weakness. Furthermore, physical examinations revealed neither muscular atrophy nor neurologic abnormalities. However, laboratory examinations detected an elevated serum intact PTH level, although serum calcium level was within the normal range (Table 1). Thus, the brother was also suspected as having PHP-Ib. The brother manifested mildly elevated serum 1,25(OH)2D level.

The 50-year-old father and 17-year-old sister were clinically normal. The mother, deceased at 49 years of age of an unknown cause, allegedly had no clinical symptoms indicative of PHP. Endocrine studies revealed no abnormalities in the father, sister, or mother (Table 1).

Molecular analyses

This study was approved by the Institutional Review Board Committee at the National Center for Child Health. After obtaining written informed consent, we extracted genomic DNA from leukocytes of the patient and his brother and father.

We examined mutations in the coding region of *GNAS* by direct sequencing, and copy number alternations and methylation defects in the *GNAS*-flanking region by methylation-specific multiplex ligation-dependent probe amplification (MS-MLPA), using a commercially available probe mix (SALSA MLPA kit, ME031-A1) (MRC-Holland, Amsterdam, The Netherlands). To confirm the results of MS-MLPA, we performed PCR analyses using forward and reverse

Table 1 Laboratory findings of the patient and his family members

	Patient	Brother	Father	Mother	Sister	Reference range
Age at the examinations (years)	12	15	50	43	17	
Height (cm) (SDS)	161.4 (+1.1)	171 (+0.1)	N.A.	N.A.	N.A.	
Weight (kg) (SDS)	42.4 (-0.2)	53 (-0.9)	N.A.	N.A.	N.A.	
<Blood>						
Intact PTH (pg/mL)	**430**	**254**	26	44	26	10-65
Calcium (mg/dL)	**6.4**	8.9	9.3	8.7	9.2	8.5-10.2
Phosphate (mg/dL)	**9.1**	**5.2**	2.9	3.8	3.4	2.4-4.3
Magnesium (mg/dL)	1.8	2.0	N.A.	N.A.	N.A.	1.8-2.5
Na (mEq/l)	142	140	N.A.	N.A.	N.A.	135-147
K (mEq/l)	4.1	4.0	N.A.	N.A.	N.A.	3.6-5.0
Creatinine (mg/dL)	0.6	0.7	N.A.	N.A.	N.A.	0.4-1.1
Alb (g/dL)	4.9	4.5	N.A.	N.A.	N.A.	3.9-5.1
CK (IU/L)	**741**	136	N.A.	N.A.	N.A.	0-170
ALP (IU/L)	**1809** (388-1190)[a]	648 (225-680)[a]	N.A.	N.A.	N.A.	
1,25(OH)2D (pg/mL)	**69**	**79**	N.A.	N.A.	N.A.	20-60
TSH (mU/L)	**5.6**	4.1	N.A.	N.A.	N.A.	0.5-5.0
Free T4 (ng/dL)	1.0	1.0	N.A.	N.A.	N.A.	0.9-1.6
<Urine>						
Calcium/Creatinine ratio	**0.004**	**0.008**	N.A.	N.A.	N.A.	0.08-0.20
%TRP	**99.6**	**99.6**	N.A.	N.A.	N.A.	89.6-93.6
<Ellsworth-Howard test>						
Urinary phosphate (mg/2 hrs)[b]	**8.33**	N.A.	N.A.	N.A.	N.A.	≥30
Urinary cAMP (μmol/hr)[c]	**0.029**	N.A.	N.A.	N.A.	N.A.	≥1.0

The conversion factors to the international system of units (SI unit) are as follows: intact PTH 1.0 (ng/liter), serum calcium 0.25 (mmol/liter), serum phosphate 0.3229 (mmol/liter) serum magensium 0.411 (mmol/liter), serum sodium 1.0 (mmol/liter), serum potassium 1.0 (mmol/liter), serum creatine 88.4 (μmol/liter), serum albumin 10 (g/liter), serum 1,25(OH)2D 2.6 (pmol/liter), serum Free T4 12.9 (pmol/liter). Hormone values have been evaluated by the age- and sex-matched Japanese reference data; abnormal data are in bold.

[a] The values in parentheses indicate the age-and sex-matched reference laboratory data.

[b] Urinary phosphate denotes the increment of 2 hours urinary excretion of phosphate after injection of human PTH (100 unit).

[c] Urinary cAMP denote the increment of 1 hour urinary cAMP excretion after injection of human PTH (100 unit).

N.A., not analysed; CK, creatine kinase; 1,25(OH)2D, 1,25-dihydroxy vitamin D; %TRP, % tubular reabsorption of phosphate

primers that hybridize to introns 3 and 6 of *STX16*, respectively [4].

Results

Direct sequence analysis for the patient identified no mutation in the coding region of *GNAS*. However, MS-MLPA revealed decreased peak heights of probes that correspond to exons 5 and 6 of *STX16*, indicating a heterozygous deletion within *STX16*. In addition, MS-MLPA indicated hypomethylation at *GNAS* exon A/B and a normal methylation pattern of the other 3 *GNAS* DMRs (Fig. 1A, B). Subsequent PCR analyses showed the presence of a heterozygous 3 kb deletion involving exons 4-6 of *STX16* (STX16Δexons 4-6) (Fig. 1C). The microdeletion and methylation defect were also observed in the brother, but not in the father. DNA samples of the mother and the sister were not available for genetic analyses.

Discussion

We report here a Japanese patient with PHP-Ib, who was identified by general fatigue, gait disturbance, and myalgia in the lower legs. He showed muscular atrophies in the lower legs, a shortening of the bilateral Achilles' tendons, absence of deep tendon reflexes, and an elevated serum CK value. Such clinical features are indicative of neuromuscular symptoms, although a detailed neurological workup was not performed for

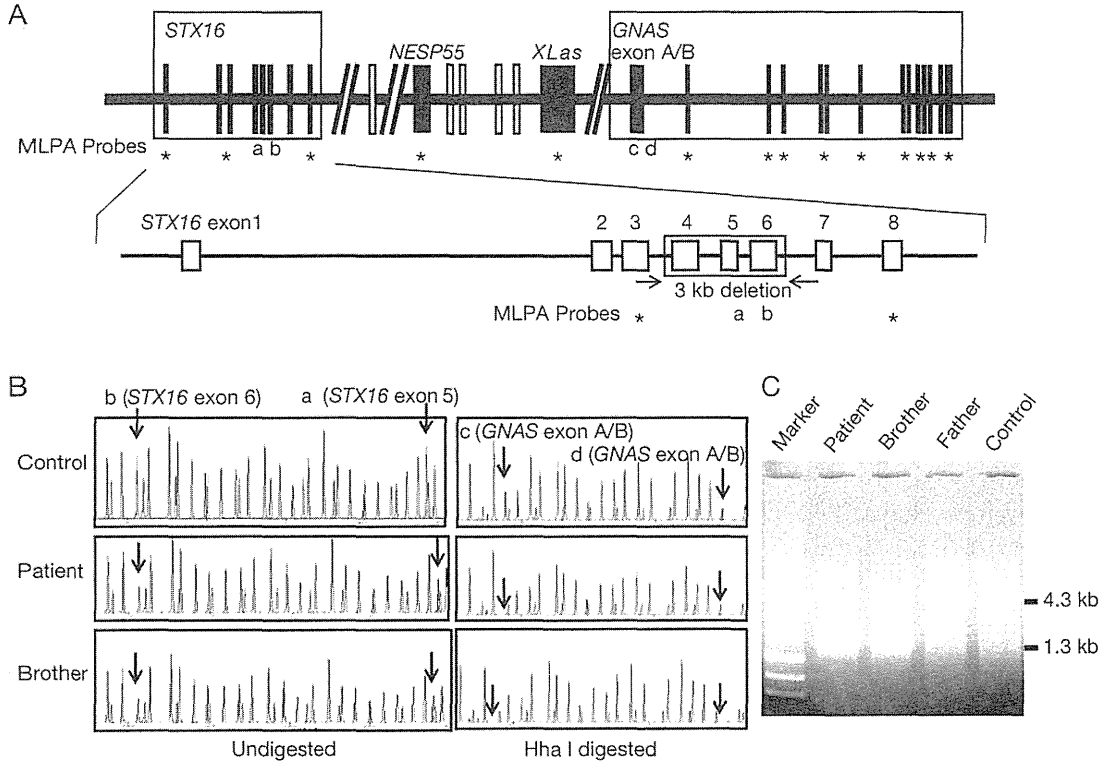

Fig. 1 Molecular analysis of the patient and his family members.
A, Schematic representation of the genomic region around *GNAS*. Upper panel: The loci examined by methylation-specific multiplex ligation-dependent probe amplification (MS-MLPA) are indicated by letters (a-d) and asterisks. Lower panel: Microdeletion identified in the patient and his brother. Horizontal arrows indicate the binding sites of the primers used for PCR analysis.
B. Representative results of MS-MLPA. Left panel: Decreased peak heights with probes a and b in the patient and his brother indicate heterozygous deletion involving exons 5 and 6 of *STX16*. Right panel: Absence of peaks with probes c and d indicate hypomethylation of *GNAS* exon A/B.
C, PCR analysis using a primer pair flanking the deletion. Both the 4.3 kb (wild-type) and 1.3 kb (STX16Δexons4-6) products were amplified from the patient and his brother, while only the 4.3 kb product was obtained from the father and the control individual.

this patient. In this regard, it is noteworthy that peripheral neuropathy and metabolic myopathy have been reported in patients with primary hypoparathyroidism [8, 9], whereas such symptoms have not been described in patients with PHP, except for mildly elevated blood CK and lactate dehydrogenase (LDH) levels in a single case of PHP-Ia [10]. Moreover, *in vitro* experiments showed that calcium concentration affects excitability at neuromuscular junctions [11]. Thus, the neuromuscular symptoms of our patient are likely to be associated with hypocalcemia. A significant improvement in the clinical features of the patient after 1 month of treatment with alfacalcidol and calcium supports this hypothesis. However, we cannot exclude the possibility that other factors such as vitamin D deficiency may also have played a role in the development of these features. Indeed, slightly elevated serum levels of ALP and 1,25(OH)2D in the patient are consistent with mild vitamin D deficiency [12]. On the other hand, since serum 1,25(OH)2D levels were similarly elevated in the patient and his asymptomatic brother, phenotypic variation in this family can not be explained by vitamin D deficiency. These results indicate that neuromuscular features probably associated with hypocalcemia can be the first symptoms of PHP-Ib. Nevertheless, this notion is based on observations of a single case, and

requires further investigations.

Both the patient and his brother carried a heterozygous STX16Δexons4-6. Although DNA samples of the mother were not available for genetic analyses, the absence of the deletion in the father indicated the maternal inheritance of the deletion. It has been shown that maternally inherited STX16Δexons4-6 (STX16Δexons4-6mat) is associated with hypomethylation at *GNAS* exon A/B, whereas *GNAS* epimutations are usually accompanied by methylation defects not only at exon A/B but also at other *GNAS* DMRs [3, 7]. These results suggest that the 3 kb region around exon 4-6 of *STX16* contains a cis-acting element that regulates methylation status at *GNAS* exon A/B. Consistent with this, our patient and his brother had methylation defects exclusively at exon A/B. Further studies are necessary to clarify the mechanism by which a DNA element >200 kb from *GNAS* controls the methylation status at exon A/B.

Clinical severities of patients with PHP-Ib are known to be variable [6, 7]. Notably, Linglart *et al.* have shown that STX16Δexons4-6mat is often associated with a mild phenotype. They found that about 40% of patients carrying this microdeletion remained asymptomatic, and more than 50% of asymptomatic individuals had normocalcemia at the time of diagnosis [7]. Consistent with this, our patient and his brother lacked typical PHP-Ib features such as tetany, generalized convulsions, or muscle cramps. Furthermore, the brother had normocalcemia. These results suggest that physical examinations and measurement of serum calcium levels are not sufficient to identify patients with PHP-Ib, and that genetic analyses or detailed endocrine evaluations, such as measurement of intact PTH levels and an Ellsworth-Howard test, are necessary for patients with atypical manifestations. In this context, although STX16Δexons4-6mat is the most frequent genetic cause of familial PHP-Ib [7], microdeletions affecting *NESP55* as well as epimutations of *GNAS* DMR also account for etiology of PHP-Ib [5, 7]. Since MS-MLPA is capable of detecting both copy number abnormalities and methylation defects in the *GNAS*-flanking region in a single assay, this method should be particularly useful for the molecular diagnosis of PHP-Ib.

In summary, the present study provides that various neuromuscular features probably associated with hypocalcemia can be the first symptoms of PHP-Ib, and suggests that MS-MLPA serves as a powerful tool for screening of *GNAS* abnormalities in patients with atypical manifestations.

Acknowledgments

We thank Dr. K. Kanno (Ojiya General Hospital) for providing us the blood samples of the family. We are also grateful to Ms. T. Tanji and E. Suzuki (National Research Institute for Child Health and Development) for their technical assistance, and Dr. J. Tohyama (Department of Pediatrics, Epilepsy Center, Nishi-Niigata Chuo National Hospital) for his fruitful discussion.

References

1. Levine MA (2000) Clinical spectrum and pathogenesis of pseudohypoparathyroidism. *Rev Endocr Metab Disord* 1: 265-274.
2. Weinstein LS, Yu S, Warner DR, Liu J (2001) Endocrine manifestations of stimulatory G protein alpha-subunit mutations and the role of genomic imprinting. *Endocr Rev* 22: 675-705.
3. Liu J, Litman D, Rosenberg MJ, Yu S, Biesecker LG, et al. (2000) A GNAS1 imprinting defect in pseudohypoparathyroidism type IB. *J Clin Invest* 106: 1167-1174.
4. Bastepe M, Frohlich LF, Hendy GN, Indridason OS, Josse RG, et al. (2003) Autosomal dominant pseudohypoparathyroidism type Ib is associated with a heterozygous microdeletion that likely disrupts a putative imprinting control element of GNAS. *J Clin Invest* 112: 1255-1263.
5. Bastepe M, Frohlich LF, Linglart A, Abu-Zahra HS, Tojo K, et al. (2005) Deletion of the NESP55 differentially methylated region causes loss of maternal GNAS imprints and pseudohypoparathyroidism type Ib. *Nat Genet* 37: 25-27.
6. Kinoshita K, Minagawa M, Takatani T, Takatani R, Ohashi M, et al. (2011) Establishment of diagnosis by bisulfite-treated methylation-specific PCR method and analysis of clinical characteristics of pseudohypoparathyroidism type Ib. *Endocr J* 58: 879-887.
7. Linglart A, Gensure RC, Olney RC, Juppner H, Bastepe M (2005) A novel STX16 deletion in autosomal dominant pseudohypoparathyroidism type Ib redefines the

boundaries of a cis-acting imprinting control element of GNAS. *Am J Hum Genet* 76: 804-814.
8. Kruse K, Scheunemann W, Baier W, Schaub J (1982) Hypocalcemic myopathy in idiopathic hypoparathyroidism. *Eur J Pediatr* 138: 280-282.
9. Goswami R, Bhatia M, Goyal R, Kochupillai N (2002) Reversible peripheral neuropathy in idiopathic hypoparathyroidism. *Acta Neurol Scand* 105: 128-131.
10. Piechowiak H, Grobner W, Kremer H, Pongratz D, Schaub J (1981) Pseudohypoparathyroidism and hypocalcemic "myopathy". A case report. *Klin Wochenschr* 59: 1195-1199.
11. Elmqvist D, Feldman DS (1965) Calcium dependence of spontaneous acetylcholine release at mammalian motor nerve terminals. *J Physiol* 181: 487-497.
12. Bringhurst FR, Demay MB, Kronenberg HM (2011) Hormones and disorders of mineral metabolism. In: Melmed S, Polonsky KS, Larson PR, Kronenberg HM (ed). Williams Textbook of endocrinology (12th). Saunders, Philadelphia: 1237-1304.

PRKAR1A Mutation Affecting cAMP-Mediated G Protein-Coupled Receptor Signaling in a Patient with Acrodysostosis and Hormone Resistance

Keisuke Nagasaki, Tomoko Iida, Hidetoshi Sato, Yohei Ogawa, Toru Kikuchi, Akihiko Saitoh, Tsutomu Ogata, and Maki Fukami

Department of Molecular Endocrinology (K.N., T.O., M.F.), National Research Institute for Child Health and Development, Tokyo 157-8535, Japan; Division of Pediatrics (K.N., H.S., Y.O., T.K., A.S.), Department of Homeostatic Regulation and Development, Niigata University Graduate School of Medical and Dental Sciences, Niigata, 951-8510, Japan; Department of Pediatrics (T.I.), Niigata National Hospital, Niigata, 945-8585, Japan; and Department of Pediatrics (T.O.), Hamamatsu University School of Medicine, Hamamatsu 431-3192, Japan

Context: Acrodysostosis is a rare autosomal dominant disorder characterized by short stature, peculiar facial appearance with nasal hypoplasia, and short metacarpotarsals and phalanges with cone-shaped epiphyses. Recently, mutations of *PRKAR1A* and *PDE4D* downstream of *GNAS* on the cAMP-mediated G protein-coupled receptor (GPCR) signaling cascade have been identified in acrodysostosis with and without hormone resistance, although functional studies have been performed only for p.R368X of *PRKAR1A*.

Objective: Our objective was to report a novel *PRKAR1A* mutation and its functional consequence in a Japanese female patient with acrodysostosis and hormone resistance.

Patient: This patient had acrodysostosis-compatible clinical features such as short stature and brachydactyly and mildly elevated serum PTH and TSH values.

Results: Although no abnormality was detected in *GNAS* and *PDE4D*, a novel *de novo* heterozygous missense mutation (p.T239A) was identified at the cAMP-binding domain A of *PRKAR1A*. Western blot analysis using primary antibodies for the phosphorylated cAMP-responsive element (CRE)-binding protein showed markedly reduced CRE-binding protein phosphorylation in the forskolin-stimulated lymphoblastoid cell lines of this patient. CRE-luciferase reporter assays indicated significantly impaired response of protein kinase A to cAMP in the HEK293 cells expressing the mutant p.T239A protein.

Conclusions: The results indicate that acrodysostosis with hormone resistance is caused by a heterozygous mutation at the cAMP-binding domain A of *PRKAR1A* because of impaired cAMP-mediated GPCR signaling. Because *GNAS*, *PRKAR1A*, and *PDE4D* are involved in the GPCR signal transduction cascade and have some different characters, this would explain the phenotypic similarity and difference in patients with *GNAS*, *PRKAR1A*, and *PDE4D* mutations. ***(J Clin Endocrinol Metab* 97: E1808–E1813, 2012)**

Acrodysostosis is a rare autosomal dominant disorder characterized by short stature, peculiar facial appearance with nasal hypoplasia, short metacarpotarsals and phalanges with cone-shaped epiphyses, and variable degrees of mental retardation (1, 2). Recent studies have shown that acrodysostosis is caused by mutations of *PRKAR1A* (protein

ISSN Print 0021-972X ISSN Online 1945-7197
Printed in U.S.A.

doi: 10.1210/jc.2012-1369 Received February 9, 2012. Accepted May 25, 2012.
First Published Online June 20, 2012

Abbreviations: AHO, Albright's hereditary osteodystrophy; CRE, cAMP-responsive element; CREB, CRE-binding; DMR, differentially methylated regions; GNAS, stimulatory G protein α-subunit; GPCR, G protein-coupled receptor; PDE4D, phosphodiesterase 4D, cAMP-specific; PHP-Ia, pseudohypoparathyroidism type Ia; PKA, protein kinase A; PRKAR1A, protein kinase, cAMP-dependent, regulatory type 1,α; RIα, type 1α regulatory subunit.

kinase, cAMP-dependent, regulatory type 1,α) and *PDE4D* (phosphodiesterase 4D, cAMP-specific) involved in the cAMP-mediated G protein-coupled receptor (GPCR) signaling cascade (3–5). *PRKAR1A* consists of 11 exons and encodes type 1α regulatory subunit (RIα) of protein kinase A (PKA) with a dimerization domain, an inhibitory site, and two cAMP-binding domains A and B (6). The PKA holoenzyme is a tetramer consisting of two regulatory subunits and two catalytic subunits, and cooperative binding of two cAMP molecules to each regulatory subunit leads to the dissociation of the catalytic subunits from the regulatory subunits (7). The regulatory subunit-associated catalytic subunits remain inactive, whereas the free catalytic subunits released from the regulatory subunits can phosphorylate a variety of substrate proteins including the cAMP-responsive element (CRE)-binding (CREB) protein (7, 8). It is likely, therefore, that the *PRKAR1A* mutations hinder the cAMP-mediated dissociation of the catalytic subunits from the regulatory subunits, thereby leading to reduced PKA signaling (3). *PDE4D* comprises 15 exons and encodes cAMP-dependent phosphodiesterase 4D (PDE4D) that regulates intracellular cAMP concentrations by converting cAMP to AMP (9). Thus, the *PDE4D* mutations appear to result in desensitization to cAMP because of persistently elevated intracellular cAMP concentrations, thereby affecting the cAMP-mediated GPCR signaling cascade (4). However, functional studies have been performed only for the *PRKAR1A* p.R368X mutation that resides on the last exon and is predicted to escape nonsense-mediated mRNA decay (3), whereas protein modeling analysis argues for the pathological consequences of the remaining *PRKAR1A* and *PDE4D* mutations (4, 5).

Notably, nine of 10 *PRKAR1A* mutation-positive patients and two of seven *PDE4D* mutation-positive patients identified to date exhibit resistance to PTH and/or TSH. Such clinical findings, *i.e.* acrodysostosis plus hormone resistance, overlap with those of pseudohypoparathyroidism type Ia (PHP-Ia), because PHP-Ia is associated with Albright's hereditary osteodystrophy (AHO) reminiscent of acrodysostosis and resistance to several hormones such as PTH and TSH. Indeed, although acrodysostosis and AHO have been classified as different skeletal disorders (2), it is often difficult to distinguish between acrodysostosis and AHO on the basis of clinical and radiological findings (10). Consistent with such phenotypic similarities, PHP-Ia is primarily caused by heterozygous loss-of-function mutations of *GNAS* (the stimulatory G protein α-subunit) (11) that resides in the upstream of *PRKAR1A* and *PDE4D* on the cAMP-mediated GPCR signaling cascade.

Here, we report on a novel *de novo* *PRKAR1A* mutation and its functional consequence in a patient with acrodysostosis and hormone resistance and discuss phenotypic findings in patients with *PRKAR1A*, *PDE4D*, and *GNAS* mutations.

Patients and Methods

Case report

This Japanese female patient was born to nonconsanguineous parents at 38 wk of gestation. At birth, her length was 46.5 cm (−0.75 SD) and her weight 1.81 kg (−2.8 SD). Neonatal screening tests were normal. Her gross motor milestones were somewhat delayed, with sitting alone without support at 10 months and walking alone at 21 months of age. Her stature remained below −2.0 SD of the mean.

At 3 yr and 10 months of age, she was referred to us because of short stature. Her height was 86.9 cm (−3.1 SD) and her weight 10.6 kg (−2.3 SD). She exhibited round face, nasal hypoplasia, anteverted nostrils, severe brachydactyly of the hands, and mild developmental retardation, and hand roentgenograms showed generalized shortening of the tubular bones with cone shaped epiphyses (Fig. 1A). Brain computerized tomography showed neither sc nor intracranial calcifications. Biochemical and endocrine studies revealed 1) increased serum PTH and plasma cAMP values and normal serum calcium, phosphate, and vitamin D values; 2) decreased urine calcium/creatinine ratio and normal percent tubular reabsorption of phosphate; 3) slightly elevated serum TSH value and normal free T_4 value; 4) age-appropriate serum LH and FSH values; and 5) normal GH response to GHRH stimulation (Table 1). Thus, she was suspected as having acrodysostosis with mild resistance to PTH and TSH.

The parents showed neither brachydactyly nor abnormal endocrine findings (Table 1), although the mother had short stature (144 cm, −2.6 SD).

Molecular and functional studies

We performed 1) direct sequencing for coding exons and their splice sites of *PRKAR1A*, *PDE4D*, and *GNAS*; 2) methylation analysis for four differentially methylated regions (DMR) around *GNAS*; 3) parental testing by microsatellite genotyping; 4) conservation of a substituted amino acid; 5) the forskolin-induced PKA activity of lymphoblastoid cell lines in terms of the phosphorylation status of the CREB protein using Western blot analysis; and 6) forskolin-induced PKA activity using HEK293 cells expressing the wild-type and the mutant proteins. The primers used in this study are shown in Supplemental Table 1, and the detailed methods are described in Supplemental Methods (published on The Endocrine Society's Journals Online web site at http://jcem.endojournals.org).

Results

Analysis of *PRKAR1A*, *PDE4D*, and *GNAS*

No pathological mutation was found for *PDE4D* and *GNAS*, nor was an aberrant methylation pattern detected for the DMR around *GNAS*. By contrast, a novel heterozygous missense mutation (c.715A→G; p.T239A)

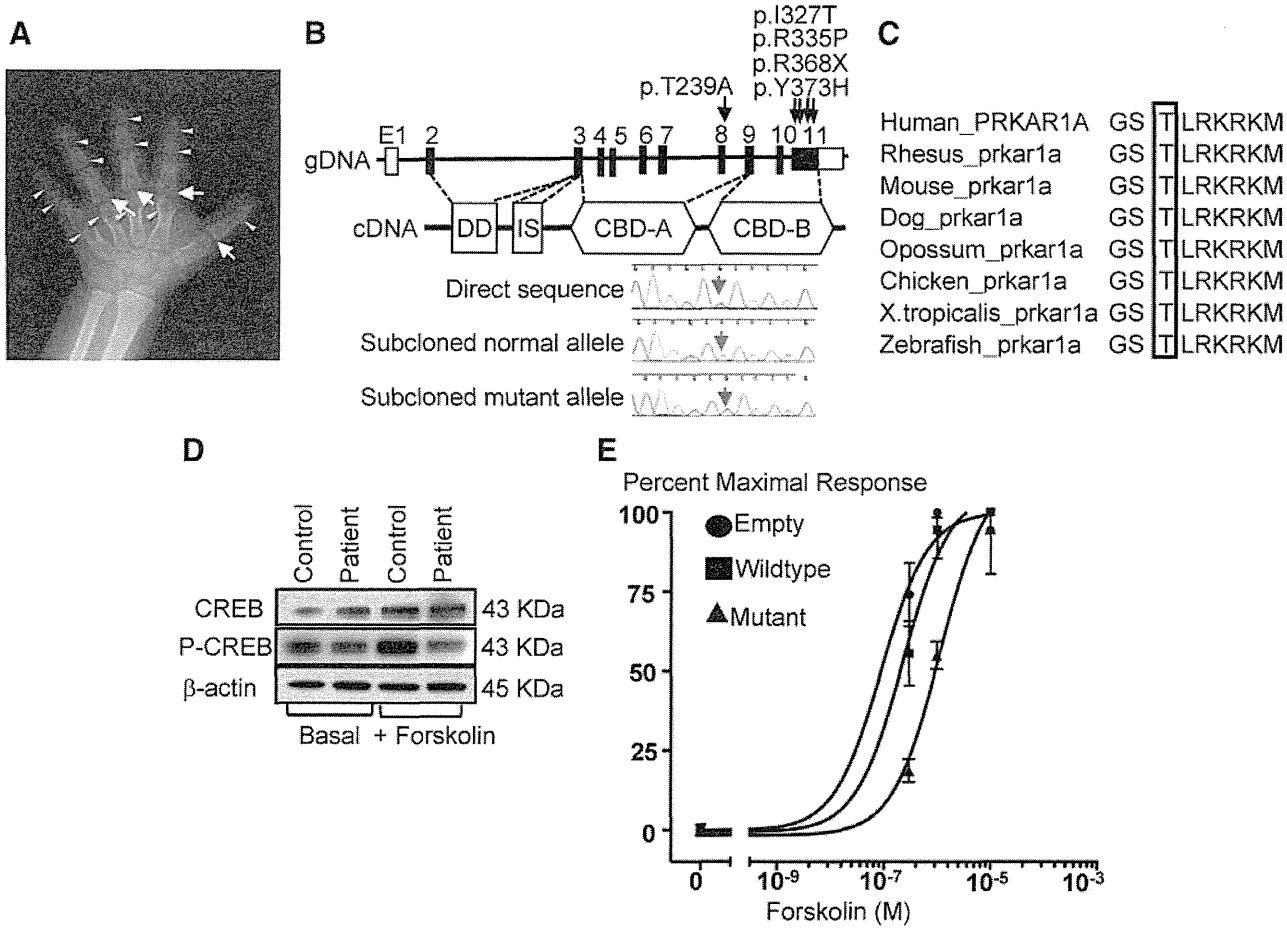

FIG. 1. Representative clinical and experimental findings of this patient. A, Radiograph of the left hand at 3 yr and 10 months of age. Note the shortening of all tubular bones with cone-shaped epiphyses (*arrows*) and early infusions (*arrowheads*). B, The structure of *PRKAR1A* and the position of the mutations identified. The *black and white boxes* on genomic DNA (gDNA) denote the coding regions on exons 2–11 and the untranslated regions, respectively. *PRKAR1A* encodes a dimerization domain (DD), an inhibitory site (IS), and two cAMP-binding domains A and B (CBD-A and -B). A missense mutation (p.T239A) was identified on exon 8 for the cAMP-binding domain A of this patient, whereas the previously described one nonsense and three missense mutations have been found on exon 11 for cAMP-binding domain B (3–5). C, Amino acid sequence of PRKAR1A. Note that the T239 residue is well conserved among species. D, Representative results of Western blot analysis for lymphoblastoid cell lines of the patient and a control subject. The cells were collected before (basal) and after stimulation with 10 μM forskolin. The samples were probed with antibodies for phospho-CREB protein (Ser 133) (P-CREB) and CREB protein, together with those for β-actin used as an internal control. E, Transactivating activities of the wild-type and the mutant PRKAR1A for the CRE-luc reporter. HEK293 cells were transfected with an empty expression vector or with vectors containing either the wild-type PRKAR1A or the p.T239A mutant. Samples were treated with various concentrations of forskolin. The values (percentages to the maximal CRE-luciferase activity) are expressed as the mean ± SE. Curves are fitted with sigmoidal dose-response models. In cells expressing the mutant protein, forskolin induced a concentration-dependent increase in CRE-luciferase activity, yet with a shift to the right in the dose-response curve. The EC_{50} values were significantly higher in the cells expressing the mutant protein than those expressing the wild-type protein ($P < 0.001$). The results are obtained from three independent experiments.

was identified on exon 8 at the cAMP-binding site A of *PRKAR1A* (Fig. 1B). This mutation was absent from her parents and 100 Japanese control subjects.

Parental testing

Microsatellite genotyping data were consistent with paternity as well as maternity of the parents (Supplemental Table 2).

Functional characterization of the mutant *PRKAR1A*

The T239 residue was well conserved among species (Fig. 1C). Protein modeling analysis indicated that the p.T239A resulted in loss of the hydrogen bond between the M236 and the T239 residues and in aberration of the random coils in the mutant PRKAR1A protein, although there was no gross conformational alteration affecting α-helices and β-strands (Supplemental Fig. 1). Western blot analysis indicated obviously reduced forskolin-induced CREB protein phosphorylation in the presence of the apparently normal amount of CREB protein in the lymphoblastoid cell line of this patient (Fig. 1D). Similarly, forskolin-induced PKA activity was significantly lower in the HEK293 cells expressing the mutant PRKAR1A protein than in those expressing the wild-type protein (Fig. 1E).

TABLE 1. Clinical and laboratory data of the patient and her parents

	Patient	Father	Mother[a]
Age (yr)	3 10/12	31	30
Height (cm) (SDS)	**86.9** (−3.1)	177 (+1.1)	**144** (−2.6)
Weight (kg) (SDS)	**10.9** (−2.3)	**89 (+2.5)**	45[b]
Blood			
Intact PTH (pg/ml)	**128** (10–65)	42 (10–65)	23 (10–65)
Calcium (mg/dl)	9.4 (8.5–10.2)	9.4 (8.5–10.2)	9.0 (8.5–10.2)
Phosphate (mg/dl)	5.6 (3.5–5.9)	3.2 (2.4–4.3)	3.6 (2.4–4.3)
25-Hydroxyvitamin D (ng/ml)	26 (7–41)	NA	NA
TSH (mU/liter)	**7.2** (0.5–5.0)	1.7 (0.5–5.0)	1.2 (0.5–5.0)
Free T_4 (ng/ml)	1.2 (0.9–1.6)	1.3 (0.9–1.6)	1.1 (0.9–1.6)
LH (IU/liter)	<0.1 (<0.7)	4.1 (0.8–5.7)	0.17 (1.8–10.2)[c]
FSH (IU/liter)	0.9 (0.6–5.3)	6.6 (2.0–8.3)	0.07 (3.0–14.7)[c]
GH (ng/ml) stimulated[d]	19.5 (>9)	NA	NA
cAMP (pmol/ml)	**39.6** (6.4–20.8)	NA	NA
Urine			
Calcium/creatinine ratio	**0.04** (0.13–0.25)	NA	NA
% TRP	91 (81.3–93.3)	NA	NA

The values in *parentheses* indicate the SD score (SDS) for heights and weights and the age-and sex-matched reference blood and urine hormone and laboratory data. The conversion factors to the SI unit are as follows: intact PTH, 1.0 (nanograms per liter); serum calcium, 0.25 (millimoles per liter); serum phosphate, 0.3229 (millimoles per liter); 25-hydroxyvitamin D, 2.496 (nanomoles per liter); free T_4, 12.9 (picomoles per liter); GH, 1.0 (micrograms per liter); and cAMP, 1.0 (nanomoles per liter). Hormone values have been evaluated by the age- and sex-matched Japanese reference data; abnormal data are in *bold*. NA, Not available; TRP, tubular reabsorption of phosphate.

[a] During the second trimester of pregnancy.

[b] Not assessed because of pregnancy.

[c] Low LH/FSH values are consistent with pregnant status of the mother (18).

[d] Blood sampling during the provocation tests were done at 0, 30, 60, 90, and 120 min after GHRH stimulation (1 μg/kg).

Discussion

We identified a novel *de novo* heterozygous *PRKAR1A* mutation in a patient with acrodysostosis and mild resistance to PTH and TSH. In this regard, several findings are noteworthy. First, although the phenotypic findings of this patient are similar to those of PHP-Ia, the severe skeletal lesion would be regarded as acrodysostosis rather than AHO. Consistent with this, a mutation was identified in *PRKAR1A* rather than *GNAS*. Second, the p.T239A was present at the cAMP-binding domain A, in contrast to the previously reported *PRKAR1A* mutations that were invariably located at the cAMP-binding domain B (3–5). In this regard, because cAMP binds first to the binding domain B and then to the binding domain A, it has been suggested that the binding domain B acts as the gatekeeper of the PKA activation, and that the binding domain A is relatively inaccessible to cAMP (8). Despite such a hierarchical phenomenon, this study indicates that mutations at the cAMP-binding domains A and B lead to a similar clinical phenotype. Third, functional analyses showed obviously reduced PKA signaling of the mutant PRKAR1A protein. Thus, the p.T239A mutation appears to impair the dissociation of the catalytic subunits from the RIα regulatory subunits, thereby leading to the reduced GPCR signaling, as has been stated by the functional studies for the p.R368X mutation (3). Although the underlying factors remains to be elucidated, loss of the hydrogen bond and aberration of the random coils in the mutant PRKAR1A protein may be relevant to this functional alteration.

To date, *GNAS*, *PRKAR1A*, and *PDE4D* mutations have been identified in patients with overlapping skeletal and endocrine phenotypes (3–5). It appears, however, that *GNAS* abnormalities usually lead to relatively mild skeletal phenotype and clinically discernible hormone resistance, whereas *PRKAR1A* and *PDE4D* mutations usually result in relatively severe skeletal lesion and mild or absent hormone resistance. In this regard, it is predicted in patients with maternally derived *GNAS* mutations that normally functioning *GNAS* is absent from several tissues including renal proximal tubules where *GNAS* is paternally imprinted and is present in a single copy in other tissues including skeletal tissues where *GNAS* is biparentally expressed (11, 12). By contrast, it is likely in patients with *PRKAR1A* and *PDE4D* mutations that normally functioning *PRKAR1A* and *PDE4D* are present in a single copy in all the tissues because of the absence of DMR around these genes (13). Such a difference in the functional gene dosage in several *GNAS*-imprinted tissues may more or less be relevant to the prevalent hormone resistance in *GNAS* mutations. Furthermore, because there are four genes encoding the regulatory subunits of PKA (RIa, RIb,